Migration Letters

Volume: 21, No: S5 (2024), pp. 1549-1558

ISSN: 1741-8984 (Print) ISSN: 1741-8992 (Online)

www.migrationletters.com

A Machine Learning Approach To Disease Prediction Using Human Aura Images

Sarika G[1], Dr. S. Palanikumar[2]

Abstract

The human body vibrates at varied rates because of several reasons. That magnetic field is the result of pulsating energy. Electrochemical processes are the basis of every biological process in the human body, from breathing and feeding to the nervous and circulatory systems. The "Bio-Energetic Field" is the result of a synthesis of magnetic and electrical energy fields. This line of inquiry has helped to shed light on a wide range of fascinating issues and characteristics that may be used to human bio-field research. The research in this field enables to comprehend more about the individual's mental condition, health difficulties, and other pertinent factors. There have been a number of advancements in this area that make it easier to analyze the human bio-field and bring attention to the fact that we as a species exist. In the proposed method, AURA pictures are used to detect the shifts. Preprocessing is the initial step in the Gas Discharge Visualisation (GDV) images; subsequently, Machine Learning (ML) techniques such as Support Vector Machine, Random Forest (RF), and Ensembled AdaBoost (Eada) are employed to identify, train, and classify characteristics. By utilizing the Ensembled AdaBoost method, the average accuracy of classification is enhanced.

Keywords: *Bio-field, Aura, GDV images, Machine Learning Techniques, Colour Co-occurrence Matrix (CCM)*

Introduction

The human body emits a variety of electromagnetic and electrical signals, including low-level heat, light, and sound. Transport or conversion of energy that defies chemical and physical description is also possible. Consisting of each of these emissions, the human energy field, also known as the biologic field or biofield, appears. The unique information stored in the human biofield can be exploited for disease diagnosis and prognosis. The most recent developments in biofield measurement are geared at scientific inquiry in the medical field. In order to diagnose organ and tissue dysfunctions before the onset of sickness or symptoms, it is necessary to take measurements of the biofield's various components [1]. When magnetic and electrical energies combine, a new field known as the "Bio-Energetic Field [2]" is created. The bio-energetic field that extends outward from a human body by about 4 or 5 feet is commonly referred to as the "Aura" [3]. A rainbow's primary colors can be seen in an aura. The hue and size of an individual's aura might be indicative of their emotional and physical wellbeing. Paradigms of the human body and the energy that

[1]Research Scholar, Department of Electronics and Communication Engineering, Noorul Islam College for Higher Education Thukalay.

[2] Former Associate Professor, Department of Information and Technology, Noorul Islam College for Higher Education, Thukalay.

sustains them. In Figure 1 we see the 122 minor and 7 major chakras that make up the human body. Any disruption to the normal functioning of the Meridian System and Chakras will have an effect on the aura that envelopes our body.

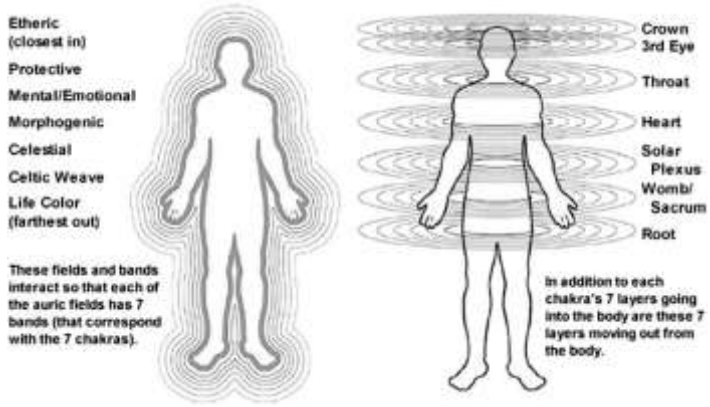

Figure 1: Chakra locations and the body's aura [4]

Medical biometric systems have been developed to address health issues and deliver top-notch healthcare. Human characteristics are extracted from a variety of media, including images, signals, and other documentation. The electromagnetic characteristics of the biofield may be evaluated using a number of different methods. Currently, medical biometrics are a prominent issue in our society because of the growing need for automated illness detection. While some biometric technologies claim instantaneous findings, others don't. The objective of this study was to monitor the progression of diseases within a healthy population through the utilization of the GDV device, which is an Electrophoton Capture (EPC) sensor designed to detect biophoton emissions originating from an individual's aura [6-8]. A prospective computerized biophysical evaluation of an individual's psychophysiologic status is provided by the GDV instrument [9]. Using GDV-based biometrics, the electro-photonic emission of patients prior to and following physical therapy, medical procedures such as spinal manipulation, spinal manipulation with acupuncture, and spinal manipulation with SOQI, chemotherapy, and energy healing have been evaluated and compared. study conducted previously utilizing Early in the progression of a disease, it might be capable of detecting deviations from normal functional status and monitoring the process of recovery to normal functioning [9]. The purpose of GDV is to use the user's fingers to assess the user's current level of psychological and physiological well-being [10]. In contrast to other biometric methodologies, the GDV biometric technology prioritizes the capture of biological patterns for medical safety.

In most cases, texture analysis makes use of the Grey Level Co-occurrence Matrix (GLCM) technique. There is little established knowledge [11] about the connection between color data and gray-GLCM texture properties. To add insult to injury, the gray-GLCM textural characteristics often show global flexibility but lack local optimisation. Shearer [12] suggested a different approach to texture analysis, one that utilizes color rather than the standard grey scale. Image processing for agricultural commodities has often made use of well-established color spaces like RGB, HSL, HSV, and L*a*b* [13]. Each person's perception of color is different, hence the HSL, HSV, and L*a*b* color spaces were developed to account for this. The CCM technique for color texture analysis is founded on the premise that color information from the visible spectrum imparts additional properties to images compared to the conventional greyscale representation. Numerous studies [14–19] have demonstrated the advantages of incorporating texture analysis into biosensing techniques.

Recent studies by Shulginov. A. and Stadnik. O. S. [20] have shown the importance and historical background of these hand-drawn and painted motifs. To establish their research's scientific validity, the authors developed and deployed an algorithm based on an image processing strategy. Colour, shape, and outline are all components of an aura picture, as discovered by the researchers. Following this, we utilized the HSV colour space to characterize the aura's color space, and last, we used a histogram derivative of the aura's intensity to establish its shape. Human biofield data was studied by Gunjan et al. [21] to determine its role in future medical diagnosis. Authors used image processing and AI techniques to create and build an algorithm for observing and interpreting a person's aura colour patterns, which are very complex and dynamic. A digital photograph was taken of the subject, and pre-processing techniques were used to eliminate background noise. They improved the image's quality by altering the contrast and luminosity of the image using image enhancement and normalization techniques. In order to depict the aura of the subject, the original RGB photograph was converted to grayscale. Subsequently, a machine learning technique was employed to identify the seven primary chakras depicted in the image. By utilizing machine learning methods, the numerical values of colors in this newly mapped color space from the RGB color model are determined. Finally, a forecasted report was made using linear regression, outlining how various colors affected the corresponding bodily systems to each chakra.

According to this research, GDV pictures might be used to diagnose the illness. Descriptors for photographs allow them to communicate more effectively. Aspects of this complexity are mined for information. Images that are adequately categorized based on them are images that are suitable for display. SVM, RF, and Eada method are used to research training and classification. This study uses GDV pictures as a first step in diagnosing sickness in the human body. Below is the outline of the rest of the paper. In Section II, we will go over the research approach that will be used, in Section III, we will go over the results of the system, and in Section IV, we will go over the research findings and recommendations for future work.

II. Methodology

Feature extraction, classification, and pre-processing were all parts of the proposed workflow. This proposed structure's high-level block diagram is shown in Figure 2. Because of the importance of adjusting the pictures for noise and contrast before feature extraction can begin, pre-processing is required.

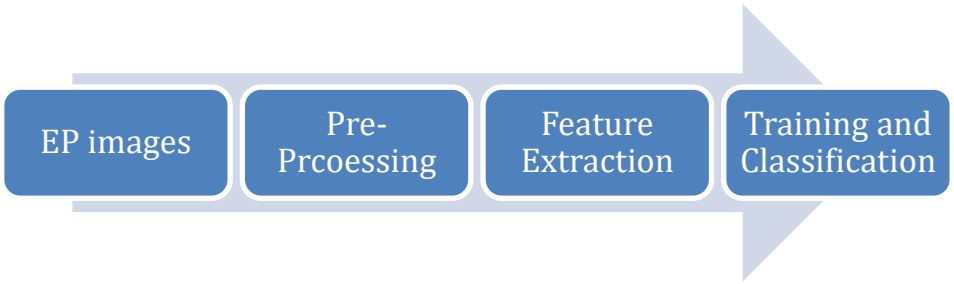

Figure 2: A schematic representation of the proposed methodology

The complete process can be delineated into three discrete phases. The initial step entails preparing the image dataset. Images are collected from various sources and then analysed. Constraints on the camera's field of view are reduced, reducing the amount of distortion shown in the final image. Resizing, smoothing, and colour adjustments are all examples of pre-processing techniques used in this approach. The photos are then prepared for feature extraction. The preprocessed image is partitioned into a training dataset and a test dataset prior to feature extraction. The model undergoes verification by means of a test set after being constructed with a training set. The models are then balanced and evaluated using the

training data. The essence of the extraction function is to pick the most important features of the data and display them in a more manageable form. The extracted picture combines a set of features into a vector. Disease prediction results are compared between the training and testing stages using Random Forest.

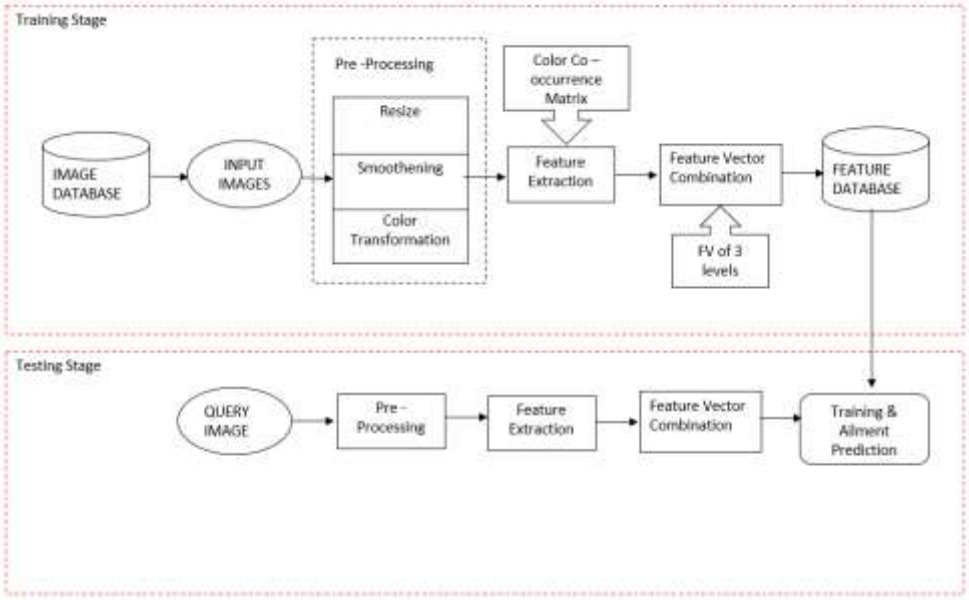

Figure 3 : A schematic representation of the proposed system's Training and Testing Phase

A) Pre-Processing

When talking about photographs, "pre-processing" refers to the rudimentary steps that are taken. Both the input and the output are intensity pictures. An intensity picture can frequently be expressed as a matrix of brightness values for image functions, so the recognized images are indistinguishable from the original sensor data. Pre-processing is done to enhance the picture data by eliminating unintended distortions and boosting specific image properties needed for smoothing. Resizing techniques are used as a preparation approach before analyzing large datasets. In the proposed study, color transformation is the key pre-processing technique. Foreground and background are utilized to their full potential. At 24 bits per pixel (8 for each RGB value), the number of potential colors in a plane is 16,777,216 (256 * 256 * 256). A color of 0 to 360 corresponds to blue, 120 to green, and 240 to red. Color purity increases with increasing saturation, with a range from 0 to 208. The value ranges from around 0 to 512, with higher values indicating brighter colors. The brightness levels of the picture are between [0, 100], where [0] is dark and [100] is white. As L increases, the hues become more vivid. The percentage of red and green tones in a picture is denoted by the letter 'A'. An intensely positive 'A' value denotes a reddish-magenta hue. The color green has a negative 'A' value, hence it's considered a negative hue. The values of 'A' can be anything, but most of the time they are in the range [-100, 100] to [-128, 127]. The amount of yellow or blue in the picture. When the value of 'B' is very high, yellow is shown. A very large negative 'B' number stands in for the color blue. Values of 'B' can be anywhere from -100 to 100, although most commonly they are between -128 and 127. Also, the luminance data is represented by a single component (Y), whereas the chrominance data is represented by two color-difference components (Cb and Cr).

B) Colour Co-occurance Matrix

The procedure of feature extraction involves the retrieval of both local and global features from an image. The features of an image are concise and direct descriptions of the data contained within it. The CCM method comprises the following three significant mathematical operations: (1) Various conversions are performed on the image, including RGB to grey [22], HSL to HSV [23], L*a*b* to XYZ [24], LCH to Luv [25], and CMY to CMYK [26]. (2) Spatial Gray-Level Dependence Matrices (SGDMs) are computed, yielding one colour space model for each colour space, and (3) fifteen Haralick textural features (TFs) are recognised [27].

Angular Second Moment (ASM)

$$f_1 = \sum_{a=0}^{N_g-1} n^2 \sum_{b=0}^{N_g-1} P_{d,\theta}(x,y)^2$$

1) Contrast:

$$f_2 = \sum_{n=0}^{N_g-1} n^2 \sum_{\substack{x=1 \\ |x-y|=n}}^{N_g} \sum_{y=1}^{N_g} \{ p(x,y) \}^2$$

2) Entropy:

$$f_3 = -\sum_x \sum_y p(x,y) \log (p(x,y))$$

3) Variance:

$$f_4 = \sum_x \sum_y (x-\mu)^2 \; p(x,y)$$

4) Correlation:

$$f_5 = \sum_{x=1}^{N_g} \sum_{y=1}^{N_g} \frac{(x,y)p(x,y) - \mu_a \mu_b}{\sigma_a \sigma_b}$$

Where μ_a, μ_b, σ_a and σ_b are the means and standard deviations of the partial probability density function $p_a p_b$.

5) Inverse difference moment (IDM)

$$f_6 = \sum_{x=0}^{N_g-1} \sum_{y=0}^{N_g-1} \frac{1}{1+(x-y)^2} P_{d,\theta}(x,y)^2$$

6) Sum Average:

$$f_8 = \sum_{x=2}^{2N_g} x \, P_{a+b}(x)$$

$P_{a+b}(x)$ is the probability of co-occurrence matrix coordinates totalling a+b and a as well as b are the co-occurrence matrix coordinates of an entry.

7) Sum Variance:

$$f_9 = \sum_{x=2}^{2N_g} (x-f_8)^2 \, P_{a+b}(x)$$

8) Sum Entropy:

$$f_{10} = -\sum_{n=0}^{2N_g} P_{a+b}(x)\log\{ P_{a+b}(x)\}$$

9) Correlation Information Measures 1:

$$f_{17} = \frac{HXY - HXY1}{\max\{HX, HY\}}$$

10) Correlation Information Measures 2:

$$f_{18} = (1 - \exp[-2.0(HXY2 - HXY)])^2$$

$$HXY = -\sum_x \sum_y p(x,y)\log\big(p(x,y)\big)$$

Where HX and HY are the entropies of P_a and P_b, respectively, and

$$HXY1 = -\sum_x \sum_y p(x,y)\log\{P_a(x)P_b(y)\}$$

$$HXY2 = -\sum_x \sum_y P_a(x)P_b(y)\log\{P_a(x)P_b(y)\}$$

11) Dissimilarity:

$$f_6 = \sum_x \sum_y |x - y| \ . \ p(x,y)$$

12) Maximum Probability

$$f_{14} = \max_{x,y} p(x,y)$$

13) Energy:

$$f_1 = \sum_x \sum_y \{p(x,y)\}^2$$

Here are some brief explanations of several textures: The entropy of a gray-level distribution is a measure of its randomness, while the energy measures the frequency with which adjacent gray-level values are paired; contrast is used to characterize the local contrast image. The homogeneity between two pixels is a measure of their local consistency. The variance measures how dispersed the greyscale values are whereas the sum mean provides the average grey level. The dominant pixel pair is the one with the highest probability, and the smoothness of the image is described by the IDM, while the cluster tendency measures the tendency for pixels of similar gray levels to cluster together. Statistically suitable paraphrase of a textual study of a biological entity.

C) Automatic Ailment Prediction

In machine learning, a classifier algorithm is used to automatically categorize input into one or more predefined categories, or "classes." Machine learning algorithms can aid automate activities that once needed manual labour. There's potential for significant cost savings and increased productivity for businesses. Here, we evaluate the suggested strategy in contrast to SVM and RF classifiers. A confusion matrix is a table that is often used to describe the performance of a classification model (or "classifier") on a set of test data for which the true values are known. Table 1 depicts the measures taken for alignment prediction where True Positive (TP) means Un-healthy medium is correctly classified as Un-healthy. False Negative (FN) means healthy medium is wrongly classified as un-Healthy. True Negative (TN) means Healthy medium is correctly classified as Healthy. False Positive (FP) means un-Healthy medium is wrongly classified as healthy.

Table 1: Alignment Prediction Evaluation Measures

Measure	**Definition**
Precision	$\frac{n(TP)}{(n(TP) + n(FP))}$
Recall	$\frac{n(TP)}{(n(TP) + n(FN))}$
Specificity	$\frac{n(TN)}{(n(TN) + n(FP))}$
Accuracy	$\frac{n(TP) + n(TN)}{n(TP) + n(TN) + n(FP) + n(FN)}$

III Results and Discussion

The process of feature extraction is implemented on a preprocessed image. For each individual plane in the input image, sixteen FV are calculated. The RGB image's feature vector has the identical dimensions to FV1 [(1x16), (1x16), (1x16)], which is 1x48. Depicting the color adjustment is Figure 4, in which a) denotes the source image and 4 signifies the outcome. Illustrative of the outcomes of the color-space translation are figures (b) through (e). To assess the efficacy of the SVM, RF, and Eada classifiers, the following metrics were calculated: precision, recall, specificity, and accuracy. The illustration of the RF classifier can be found in Table 3, whereas the Eada classifier is presented in Table 4. Table 2 presents the performance metrics pertaining to each color space transformation. Table 5 displays the values of the global performance parameters corresponding to each classifier. The findings pertaining to the assessment of the effectiveness of SVM, RF, and Eada are illustrated in Figure 6.

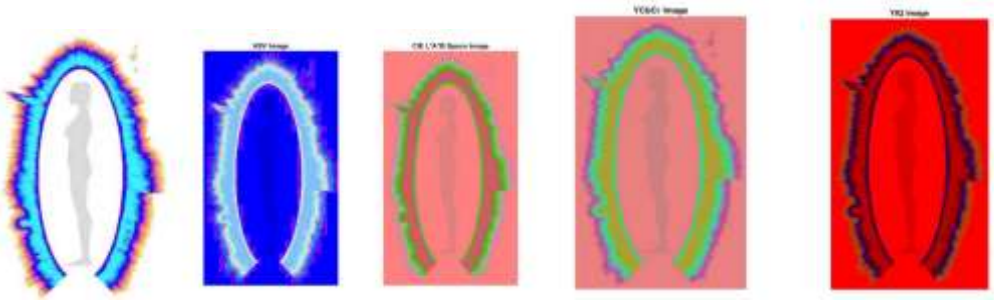

(a) (b) (c) (d) (e)

Figure 4: Output of Colour space Transformation

a) input image b) HSV image c) CIE L*a*b space image d) YCbCr image e) YIQ image

Table 2: Performance parameters value of SVM classifier for different Colour space Transformations

SVM Evaluation	**RGB**	**HSV**	**L*a*b**	**YCbCr**	**YIQ**

Precision	0.62	0.58	0.67	0.71	0.73
Recall	0.74	0.72	0.79	0.82	0.87
Specificity	0.11	0.1	0.21	0.28	0.37
Accuracy	0.53	0.49	0.6	0.65	0.7

Table 3: Performance parameters value of RF classifier for different Colour space Transformations

Random Forest Evaluation	**RGB**	**HSV**	**L*a*b**	**YCbCr**	**YIQ**
Precision	0.67	0.62	0.71	0.76	0.78
Recall	0.79	0.78	0.84	0.85	0.9
Specificity	0.21	0.19	0.32	0.35	0.44
Accuracy	0.6	0.56	0.67	0.7	0.75

Table 4: Performance parameters value of Eada classifier for different Colour space Transformations

Ensembled Adaboost Evaluation	**RGB**	**HSV**	**L*a*b**	**YCbCr**	**YIQ**
Precision	0.79	0.72	0.82	0.82	0.89
Recall	0.83	0.8	0.9	0.85	0.99
Specificity	0.3	0.14	0.42	0.38	0.67
Accuracy	0.68	0.8	0.75	0.74	0.89

Table 5: Overall performance parameters value for different classifiers

Classifier Evaluation	**SVM**	**RF**	**Eada**
Precision	0.75	0.79	**0.88**
Recall	0.88	0.92	**0.99**
Specificity	0.38	0.44	**0.66**
Accuracy	0.8	0.75	**0.89**

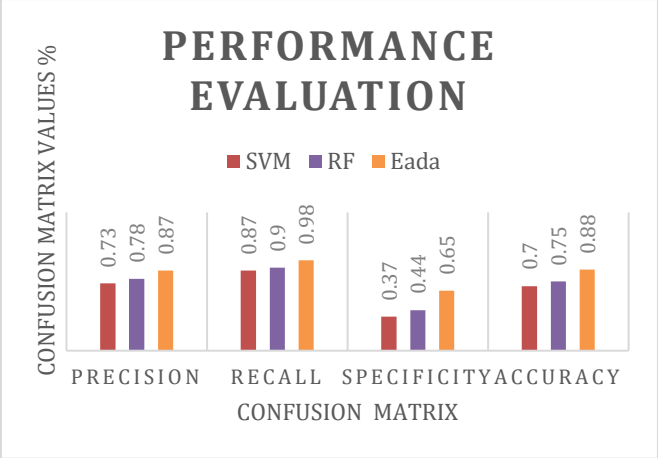

Figure 5 : Performance Evaluation graph for SVM, RF and Eada.

The tables and figures demonstrate that the SVM has an accuracy of 70%, the RF has an accuracy of 75%, and the proposed method, the Eada classifier, has an accuracy of 88%. When compared to the current algorithm, the proposed method was shown to be more effective.

IV. Conclusion and Future prospects

Medical biometrics is a branch of biometrics that focuses on illness diagnosis. Images captured by the GDV's AURA instrument will be analysed to pinpoint the discrepancies. In order to detect a medical illness in its early stages—which manifest as an increase in entropy and divergence from the usual operating state—GDV may be able to match the present needs of medical biometrics. Colour information in this work can be represented in a variety of color spaces, including HSV, L*a*b, YCbCr, etc. The use of CCM with varying distance and direction can result in more complete feature extraction. The prediction model was initially introduced using a wide variety of feature combinations and popular categorization techniques. The Ensembled AdaBoost model performed the best in terms of disease prediction accuracy (88 percent). In order to enhance the precision of disease forecasting, future studies should concentrate on creating more advanced ML algorithms. Together, ROI detection and a number of segmentation methods can pinpoint the precise organ or body part at risk. In addition, expanding databases on different demographics is necessary for computing the energy and balance. To conclude, better feature selection procedures should be implemented to boost the performance of the learning models.

References

[1] Beverly Rubik, “Measurement of the Human Biofield and Other Energetic Instruments”, Energetics and Spirituality by Lyn Free man, 2008.
[2] Hammerschlag R, Levin M, McCraty R, Bat N, Ives JA, Lutgendorf SK, Oschman JL. Biofield Physiology: A Framework for an Emerging Discipline. Glob Adv Health Med. 2015 Nov;4(Suppl):35-41.
[3] https://www.speakingtree.in/allslides/the-scientific-evidence-of-human-aura
[4] Chhabra, Gunjan & Prasad, Ajay & Marriboyina, Venkatadri. (2019). Comparison and performance evaluation of human bio-field visualization algorithm. Archives of Physiology and Biochemistry.
[5] International Conference on Medical Biometrics. 2010, http://www4.comp.polyu.edu.hk/~icbd/
[6] Korotkov, KG. Human energy field study with GDV bioelectrography. Fair Lawn, New Jersey: Backbone Publishing; 2002.
[7] Korotkov K, Williams B, Wisneski LA. Assessing biophysical energy transfer mechanisms in living systems: the basis of life processes. J Altern Complement Med. 2004; 10:49–57.

[8] Korotkov KG, Matravers P, Orlov DV, Williams BO. Application of electrophoton capture (EPC) analysis based on gas discharge visualization (GDV) technique in medicine: a systematic review. J Altern Complement Med. 2010; 16:13–25.
[9] Kostyuk N, Cole P, Meghanathan N, Isokpehi RD, Cohly HH. Gas discharge visualization: an imaging and modeling tool for medical biometrics. Int J Biomed Imaging.
[10] H. Cohly, N. Kostyuk, R. Isokpehi, and R. Rajnarayanan, "Bio-electrographic method for preventive health care," in Proceedings of the 1st IEEE Annual Bioscience and Biotechnology Conference, 2009.
[11] Yin M, Panigrahi S 2004 Image processing techniques for internal texture evaluation of French fries Appl. Eng. Agric. 206 803-811.
[12] Shearer S A 1986 Plant identification using colour co-occurrence matrices derived from digitized images PhD Dissertation Department of Agricultural Engineering Ohio State University Columbus Ohio USA.
[13] Das, N. And Palanikumar, S., 2020. Bilateral Filter Based Image Enhancement For Retinal Fundus Images. Oxidation Communications, 43(3).
[14] Hendrawan Y, Murase H 2010 Neural-Genetic Algorithm as feature selection technique for determining sunagoke moss water content Eng. Agric. Environ. Food (EAEF) J. 3 1 25-31
[15] Hendrawan Y, Murase H 2011 Non-destructive sensing for determining Sunagoke moss water content: Bio-inspired approaches Agric. Eng. Int.: CIGR Journal 15 64 131.
[16] Hendrawan Y, Murase H 2011 Bio-inspired feature selection to select informative image features for determining water content of cultured Sunagoke moss Expert Syst. Appl. 381 4321-14335.
[17] Hendrawan Y, Murase H 2011 Neural-intelligent water drops algorithm to select relevant textural features for developing precision irrigation system using machine vision Comput. Electron. Agric. 772 214-228.
[18] Hendrawan Y, Murase H 2011 Neural-discrete hungry roach infestation optimization to select informative textural features for determining water content of cultured Sunagoke moss Environ. Control Biol. 491 1-21.
[19] Hendrawan Y, Al Riza D F 2016 Machine vision optimization using Nature –inspired algorithms to model Sunagoke moss water status Int. J. Adv. Sci. Eng. Inform. Technol. 6 2088-5334.
[20] Shulginov.A.; Stadnik.O.S. "Recognition and Classification of Plasma Clots of Bioelectograms" 2018 Global Smart Industry Conference (Glosic), 978-1-5386-7386
[21] Gunjan Chhabra, Ajay Prasad, Venkatadrimarriboyina "Future Trends of Artificial Intelligence In Humanbiofield" International Journal Of Innovative Technology And Exploring Engineering (Ijitee) Issn: 2278- 3075, Volume-8 Issue-10, August 2019
[22] Rotterman Y, Porat M 2006 Colour image coding using regional correlation of primary colours Image Vision Comput. 25 637-651.
[23] Angulo J, Serra J 2007 Modelling and segmentation of colour images in polar representations Image Vision Comput. 25 475-495
[24] Leon K, Mery D, Pedreschi F, Leon F 2006 Colour measurement in L*a*b* units from RGB digital images Food Res. Int. 39 1084-1091
[25] Kim M C 2008 Comparative colour gamut analysis of xvYCC standard Displays 29 376-385
[26] Palm C 2004 Colour texture classification by integrative Co-occurrence matrices Pattern Recogn. 37 965-976.
[27] Hendrawan Y, Murase H 2011 Non-destructive sensing for determining Sunagoke moss water content: Bio-inspired approaches Agric. Eng. Int.: CIGR Journal 15 64 131.